This is a preprint of a paper to appear on IET Wireless Sensors Systems

IET Journals
The Institution of Engineering and Technology

Device-free indoor localisation with small numbers of anchors

ISSN 1751-8644
doi: 0000000000
www.ietdl.org

Francesco Potortì, Pietro Cassarà, Paolo Barsocchi

*CNR-ISTI, via Moruzzi 1, 56124 Pisa (IT) * E-mail: Potorti@isti.cnr.it*

Abstract: Device-free indoor localisation based on RSS is unobtrusive and cheap. In a world where most environment are rich in ubiquitous small radio transmitters, it has the potential of being used in a "parasitic" way, by exploiting the transmissions for localisation purposes without any need for additional hardware installation. Starting from state of the art, several step are needed to reach this aim, the first of which are tackled in this paper. The most promising algorithms from the literature are used to experiment in a real-world environment and with a rigorous measurement and analysis framework. Their positioning error performance is analysed versus number and position of devices. The original results obtained show that the currently available RSS-based device-free indoor localisation methods may be well suited to serve as a basis for providing a cheap localisation service in smart environments rich in IoT radio devices.

1 Introduction

Device-free indoor localisation is a fast-growing research topic. In the last few years several papers have appeared in the literature, proposing promising methods that allow to identify the position of a user in an indoor area without any need for user's cooperation, even behind walls.

Of these, we are particularly concerned with methods that detect the radio field perturbations produced by a user moving in the vicinity of small, low-power communications devices. The main interest we see in these technologies is that in the foreseeable future we envision an ever growing presence of small radio transmitters in indoor environments.

These localisation methods are capable of recognising the user position using only the Received Signal Strength (RSS), a measurement that can be readily obtained from low-cost wireless communication devices. This means that indoor localisation services can leverage the RSS exchanged among devices deployed in the environment to infer the user position and create new services. Since the RSS does not require a special or a sophisticated hardware and it is a standard feature of wireless devices, the techniques that exploit the RSS measurements are simple and minimally invasive. In a futuristic scenario, we envision an environment enriched with ubiquitous wireless devices that routinely exchange communication packets, for which measuring the RSS comes at no additional installation cost [1].

This scenario may lend itself to a "parasitic" usage of the radio transmission for localisation purposes. In other words, in perspective, we imagine a situation where the transmission of radio packets is useful for localisation purposes without the transmitters being designed for such use. Everything we need is the RSS at the receiving side. Such information is always available at the receivers, and requires no hardware changes to already existing systems.

There are two problems in this vision. While most papers in the literature are concerned with using a *high number* of *dedicated* transmitting devices [2, 3], our scenario involves a generally *small number* of devices working with possible *intermittent* operation. For example, in [4] 30 devices are used to survey a 70 m^2 area, each transmitting or receiving a packet every 3 ms. This is a scenario that makes sense for a laboratory experimentation or a dedicated, high-precision, quick-reaction system. In our perspective parasitic scenario, for example in a domestic environment, we may expect a lower density of devices; moreover, many of those may transmit only occasionally. For our vision to make sense, we then need to assess the capability of device-free systems to work with a *small number* of devices, and moreover to work with devices that may transmit and receive in an *intermittent* fashion. This paper is concerned with the first problem: the number of devices.

We present two analyses: a comparison between some device-free localisation methods based on the RSS and a study of their performance versus the number of deployed sensor nodes. The methods taken into account in this paper are one classification-based method [5] and two variations on the Radio Tomographic Imaging (RTI) method [6].

We show that RTI methods are simpler to use than the classification-based ones, because the latter require a recalibration every time the localisation environment is somehow changed. On the other side, they provide better position estimation than RTI [7].

We also show that the localisation accuracy versus the number of sensors is well-behaved down to few sensors per room, decreasing smoothly for all analysed methods.

The paper is organised as follows. Section 2 presents an overview on the RSS-based device-free indoor localisation methods presented in the literature. Sections 3 and 4 detail the experimental scenario and the algorithms analysed in this paper, respectively. Results are reported and commented in section 5, followed by conclusions and open research problems.

2 Related work

Many different technologies have been used to build passive indoor positioning systems, from capacitive sensors placed on floor tiles [8] to video cameras [9] and air pressure sensors able to detect the human movement by differential air pressure in HVAC (Heating, Ventilating and Air Conditioning) systems [10]. While these technologies require dedicated hardware, techniques that exploit the RSS do not require special devices and are minimally invasive. RSS-based device-free localisation algorithms use the RSS variation caused by the presence of users to infer their position. Some methods simply try to detect when a line-of-sight radio link between two devices becomes obstructed [11, 12], while others use more sophisticated approaches. In contrast to simpler methods based on link obstruction detection, the latter ones consider the whole set of disturbances induced by a target on all the links between pairs of devices. Two such methods are commonly used in the literature: classification and Radio Tomography Imaging (RTI).

Classification-based methods rely on estimation and classification of some features linked to the target position through the measured RSS [5], in this case machine learning and stochastic regression models are adopted. Radio tomography imaging methods apply

Fig. 1: A living room instrumented with transceivers for electric appliances.

imaging techniques to the interfering image produced by the presence of the target [6], in this case optimised inverse problems are solved to get the outcome.

In [13, 14] the authors propose an approach where the path loss and the RSS are jointly modelled based on diffraction theory Starting from a stochastic model [15] that describes the target-induced RSS perturbations. A Bayesian framework built on the model optimally exploits the location information coming from attenuation, random fading and mobility model. Since the presence of the target is shown to affect both the attenuation and the random fluctuations of the received power, a log-normal model is defined where the RSS mean and variance are expressed as functions of the target location. The increase of path-loss and power fluctuation induced by the moving target are described by exploiting the theory of diffraction: a closed-form analytical model is derived, tailored for the specific localisation problem and validated on experimental data.

In [16, 17] authors propose a device-free localisation system based on the RTI approach. A Radio Frequency Identification Device (RFID) network is deployed in the localisation area with the purpose to reduce the costs related to active sensor nodes (i.e. 802.15.4 nodes). Only few active RFID reader antennas are required, and passive transponders do not need batteries and can be easily placed in the whole room, i.e. under the carpet or wallpaper.

The authors of [18, 19] propose a nonlinear measurement model relating to user's position and use particle filtering to track the user. However, the accuracy decrease in crowd environments and computational due to the particle filtering is high.

In [20] authors use RTI with a background learning algorithm that models the effect of motion on the measures on each link of the wireless sensor network. They claim two major advantages of this method. First, the background learning algorithms adapts to time-varying environment and offline calibration is no longer needed. Second, performance of multi-target detection is increased. Two background learning algorithms are introduced and analysed: mixture of Gaussians (MoG) and kernel density estimation (KDE). Tikhonov regularisation is applied to the reconstruction of images.

In [21, 22] the authors use RTI with a kernel distance approach to quantify the change due to the target movements, rather than the change in mean or variance. Using kernel distance allows authors to locate a target who is stationary or moving, both in LOS and non-LOS environments. The approach is that mean and variance are just two aspects of a random variable, while it is possible to quantify the changes in mean, variance and other distribution features in a single metric. The authors explore different metrics including the Kullback-Leibler divergence and kernel distance, and find that the kernel distance performs better than other metrics in network RF environment sensing.

In this paper we consider one classification-based method [5] and two variations on RTI [6]. Both are explained in detail in section 4;

3 Scenario

We execute the measurement campaign in two rooms hosted within our research institute, we refer to them are as the localisation area. The rooms have a total surface of 75 m^2 (see figure 2). Some obstacles are present within the localisation area, such as a desk placed in the right lower corner of the first room, and a square formed of wooden walls in the upper centre part of the second room, so the net usable area is 59 m^2. The floor is made of square tiles of edge 60 cm. We stick on the floor a number of marks in order to draw the path that the target follows during the experiments. The marks are shown as grey crosses in figure 3. The target moves along the path by stepping over the marks, at a regular speed of one step per second, with the help of a metronome, and stays still for 5 s on the points indicated with a grey crossed circle. Since the movement of the target is precisely detailed and reproducible, creating a ground truth for measuring the localisation error is straightforward.

Anchors are the nodes of a Wireless Sensor Network (WSN) deployed in the localisation area. They gather the RSS values while the target moves along the paths. Anchors are IRIS Motes from Crossbow [23], based on the RF transceiver AT86RF230 at 2.4 GHz, compliant with IEEE 802.15.4 standard. Most anchors are hung on the room walls. Three measurements are done, using 16, 20 and 24 anchors. In figure 2 the group of 16 anchors is shown with red squares. The four black squares are added for the 20 anchors measurement, and finally the four white diamonds are added for the 24 anchors measurement. Of these, anchor number 1 is a sink node connected to a Linux-based laptop via USB, located on the desk, which collects all the RSS value information from the network but does not transmit during normal operation.

The RSS values are distributed thanks to a TinyOS application running on every node of the WSN. The protocol, inspired by the SpinQueue algorithm [24], is used to schedule node transmissions, in order to prevent packet collisions and maintain a high data collection rate. When an anchor transmits, all other anchors receive the packet and measure the received signal strength of the received packet. These RSS measurements are transmitted to the laptop base

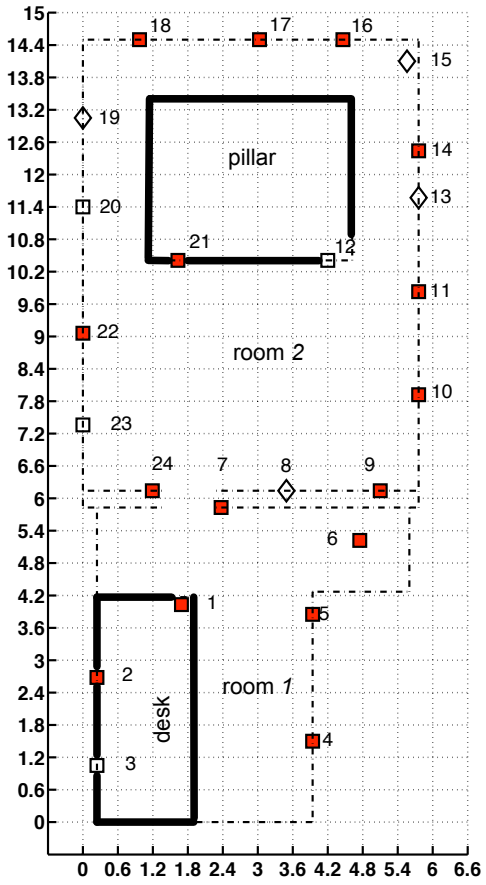

Fig. 2: Localisation area. The pillar has wooden walls, dotted lines represent the walls of the rooms. Numbered markers indicate the positions of anchors.

station along with the node's unique ID. The sink node ($i = 1$) connected to the base station collects all transmissions from the other anchors, which contain the RSS measurements, and forwards the data via USB for storage and later processing.

Each anchor is tagged with a unique index, $i = 1 \cdots n$, the protocol consists of rounds in which anchors broadcast a message in turn. At startup, the sink node ($i = 1$) broadcasts a starting message and then just listens to the network, receiving and logging the messages coming from the other anchors. Upon receiving the starting message, anchor with index 2 broadcasts the first packet. All other anchors receive the packet, perform the RSS measurement and store its value on the payload of the packet they will send next. After anchor 2 has transmitted, the next one ($i = 3$) broadcasts its packet containing all the stored RSS values, and so on until all anchors have transmitted in fixed order. The next round starts again with anchor 2, but on a different IEEE802.15.4 communication channel: four different channels are used in a round-robin fashion. After four rounds, the whole procedure is restarted.

In the real implementation, this basic sketch of the algorithm is augmented with error checking and auto-correction features based on a series of timeouts which are necessary to cope with the occasional packet loss and possible consecutive packet losses which may cause lost synchronisation in the token-passing protocol. This is necessary because the token-passing is completely distributed apart from the sending of the starting message at the beginning. Using the above described hardware, the WSN is able to send about 60 packets per second.

4 Description of algorithms

As already mentioned, we consider two approaches to the problem of device-free localisation based on the RSS, namely classification and radio tomographic. The former is based on the classification of features linked to the target position through the measures of RSS [5], the latter evaluates the interfering image produced by the user presence [6]. In the following we describe the classifier (CLAS) [5] as well as the RTI approach that comes in two flavors, namely the shadow-based radio tomographic imaging (SRTI) [4] and the variance-based one (VRTI) [25].

4.1 Classification-based method

In [5], authors propose a localisation algorithm based on the learning by example (LBE) strategy to localise and track a target. The localisation problem is addressed only by considering the available RSS values at the nodes of the wireless sensor network deployed in the localisation environment.

Each anchor $a_j,\ j = 1 \dots N$ is a transceiver located at a known position $(x_{a_j}, y_{a_j}),\ j = 1 \dots N$. Under the assumption that each node communicates with all the remaining $N - 1$ nodes, a total amount of $L = N(N - 1)$ wireless links are available. The measured value of signal strength s_j^i on the link $l = (a_i, a_j)$ depends on the interactions among the electromagnetic signal radiated by the i^{th} source, the localisation scenario, and the targets to be localised. The calibration phase of the RSS values is performed without the target in the localisation area, in order to distinguish the impact of the user movements on the RSS values from the impact of the surrounding environment. During the localisation phase the RSS values are filtered taking into account the RSS values $\hat{s}_j^i$ collected during the calibration phase. The contribution of the surrounding environment is filtered out from the RSS measures s_j^i obtained when the target is in the area, by defining a *differential measure* of the RSS values as

$$\Gamma_{ij} = \frac{s_j^i - \hat{s}_j^i}{\hat{s}_j^i},\ i = 1 \dots N,\ j = 1 \dots N - 1.$$

The differential measure is acquired for all the WSN links $\mathbf{\Gamma} = \{\Gamma_{ij},\ i = 1 \dots N,\ j = 1 \dots N - 1\}$. Starting from the differential measurements $\mathbf{\Gamma}$, the addressed problem is about the definition of the probability that the target lies in a given position $\mathbf{x} = [x, y]$ of the localisation area.

To evaluate the probability that the user lies in a given position, a classification technique based on Support Vector Machine (SVM) is adopted. SVM ([26, 27]) is a binary linear classifier, meaning that it assumes linear separability of two classes of data and attempts to find a hyperplane in the feature space separating the data points of the two classes. The optimum separation is achieved by the hyperplane that maximises its distance from the marginal data points on each side (the support vectors), that is the maximum-margin hyperplane. Thanks to the use of kernel functions, used to nonlinearly map the feature space into a high-dimensional space, computation of the hyperplane can be made using quadratic programming, a computationally efficient optimisation technique. SVM requires a learning phase, that is a preliminary system calibration procedure where a set of RSS measurements at a grid of points in the environment are collected. Points chosen for learning correspond to possible locations of the user that should be localised. For each point a tuple of RSS values is produced, and is stored in a learning database. Once the learning phase is completed, the system enters the localisation procedure, when every time a new RSS tuple is produced, the SVM uses information learned from the tuples stored in the database to classify it, that is to find the most likely position of the user.

An SVM method needs R training configurations Δ,

$$\Delta = \{(\Gamma, \mathbf{x}_m, v_m)_r,\ r = 1 \dots R\}$$

given by the set of differential measurements $\mathbf{\Gamma}$, a random position $\mathbf{x}_m$ with the associated state

$$v_m = \begin{cases} 1 & \text{if the target is in } \mathbf{x}_m \\ -1 & \text{otherwise.} \end{cases}$$

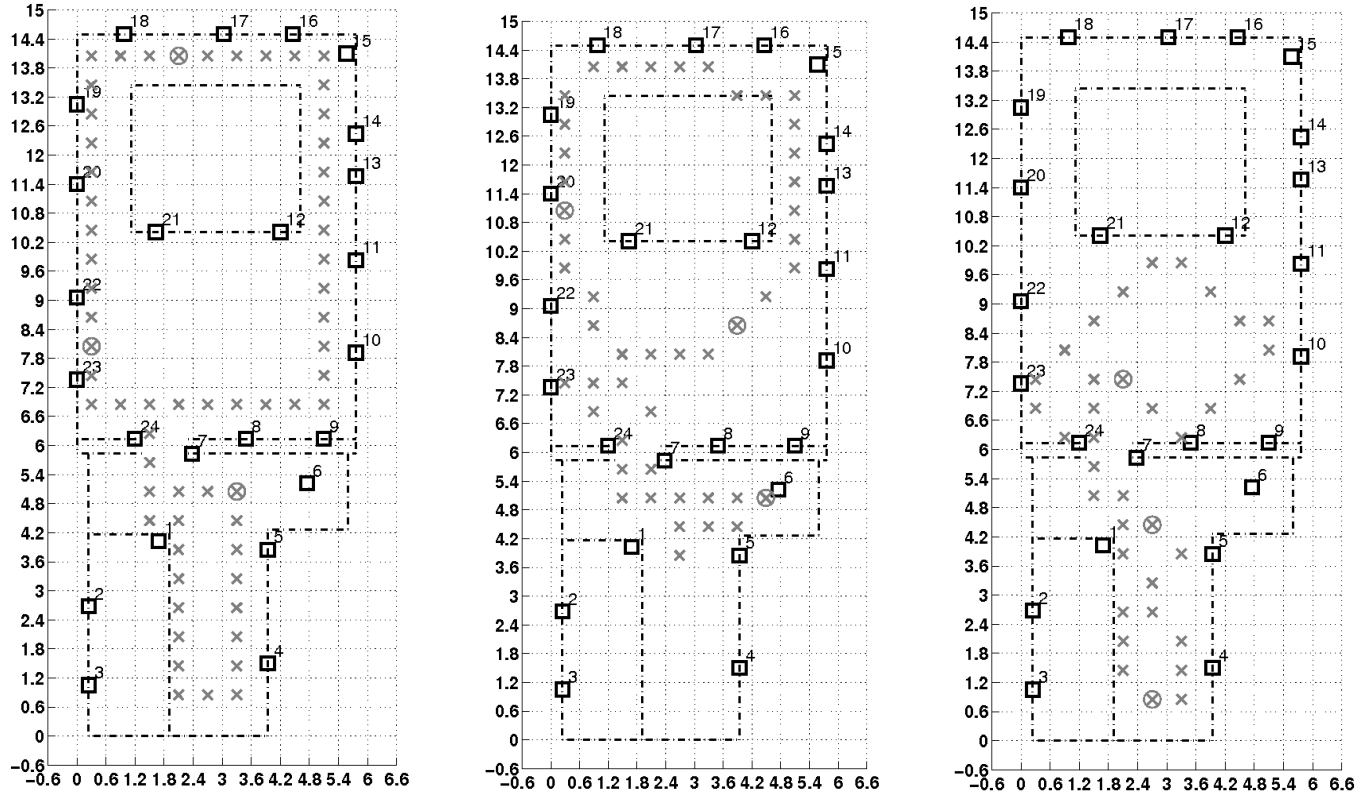

(a) Path 1 (b) Path 2 (c) Path 3

Fig. 3: Paths walked by the target user

During the training phase, the training set is used to find a suitable decision function Φ by means of an SVM strategy [26, 27]. Assuming that the localisation area is a lattice with C squared cells, the authors define the decision function for the given cell c by

$$\Phi(\mathbf{\Gamma}, v_c) = \sum_{p=1}^{C}\sum_{r=1}^{R}\left\{\alpha_c^r v_c^r \Theta(\mathbf{\Gamma}^{(r)}, \mathbf{\Gamma}^{(p)}, p, c)\right\} + \frac{\sum_{p=1}^{C}\sum_{r=1}^{R_{sv}}\left\{v_c^r - \sum_{p=1}^{C}\sum_{r=1}^{R}\left\{\alpha_c^r \Theta(\mathbf{\Gamma}^{(r)}, \mathbf{\Gamma}^{(p)}, p, c)\right\}\right\}}{R_{sv}}$$

where $\Theta(\cdot)$ is the kernel function adopted for the problem addressed, the α values are the Lagrange multipliers of the optimisation problem associated with the SVM problem, and R_{sv} is the support vector, i.e. the set of training data where the Lagrangian multipliers for the cell c are not equal to zero. Reference [28] provides an in-depth analysis of the problem. Through the decision function, the classification problem can be defined as a binary classification problem.

Note that the sign of the decision function can be replaced by the posterior probability $Pr\{\mathbf{v} = 1|\mathbf{\Gamma}\}$ [29] to construct a location-probability map of the monitored area. The posterior probability gives information about the degree of membership of test data to a particular class, even if $sign[\Phi(\mathbf{\Gamma})]$ does not correctly classify the input pattern. This behaviour is mainly due to the generalisation capabilities of the SVM approach that, in presence of highly non-separable data, constructs the best separating hyperplane even if the optimal solution to the optimisation problem [27] does not exists. In this way, the input test data could belong to the wrong half-plane identified by the decision function. However, taking into consideration the posterior probability it is still possible to compute the distance of that example to each class.

The mapping between the state information and the posterior probability can be provided by

$$Pr\{v_c = 1|\mathbf{\Gamma}\} = \frac{1}{1 + exp\left\{\gamma\Phi(\mathbf{\Gamma}, v_c) + \delta\right\}}$$

where γ and δ are obtained by resolving the optimisation problem of a cost function of the training data set, as shown in [28].

Finally the estimated target position is obtained as

$$\hat{x} = \frac{\sum_{c=1}^{C} xPr\{v_c = 1|\mathbf{\Gamma}\}}{\sum_{c=1}^{C} Pr\{v_c = 1|\mathbf{\Gamma}\}}$$

$$\hat{y} = \frac{\sum_{c=1}^{C} yPr\{v_c = 1|\mathbf{\Gamma}\}}{\sum_{c=1}^{C} Pr\{v_c = 1|\mathbf{\Gamma}\}}$$

4.2 Radio tomography method

In [6] and [4] the authors discuss the application of tomography to a wireless sensor network, calling this method Radio Tomographic Imaging (RTI). The idea behind the RTI method is that the target modifies the RSS field in a way that depends on his locations; RTI approaches, therefore, exploit the RSS measurements observed along the peer-to-peer links to obtain an image reconstruction of the object position.

In [6] the authors describe how to localise a target through the estimation of the mean RSS (SRTI), while in [25] they improve the algorithm performance by exploiting the RSS variance (VRTI) experienced during target movements. Both algorithms are here evaluated

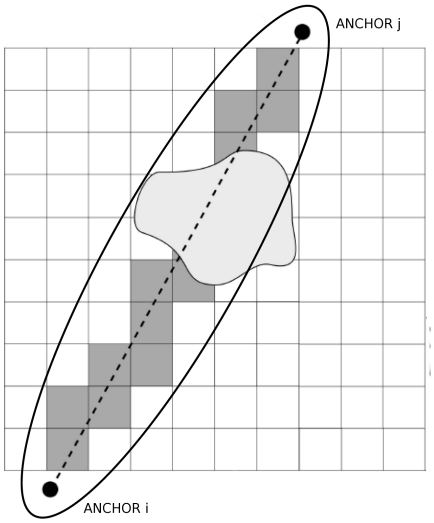

Fig. 4: Pixels affected by RSS changes due to an intervening body along the line of sight between transmitting and receiving node.

exploiting RSS measurements performed on multiple channels (i.e. frequencies) as described in [4].

The network area is conventionally divided into pixels, so the movement of the user is discretised on the pixel set.

The problem is to find a mapping that links the measured RSS per link to the RSS per pixel. The authors adopt a very simple linear model

$$\mathbf{s} = W\mathbf{s}_{px} + \mathbf{n} \tag{1}$$

where $\mathbf{s}_{px} \in \mathbb{R}^P$ is the RTI over the pixel set, so s_{px_i} is the value of RSS for the $i-th$ pixel, $\mathbf{s} \in \mathbb{R}^L$ is the vector of the measured value of RSS over the set of links, $\mathbf{n} \in \mathbb{R}^L$ is the noise of the measures, and finally $W \in \mathbb{R}^{LxP}$ is the mapping matrix whose entries are the weights that link the pixel values to the link values of RSS.

The weights of the mapping matrix W can be calculated assuming that the power of the received signal is proportional to the inverse of the squared distance covered by the signal, and that the target crossing a link (a_i, a_j) influences a set of pixels. Precisely, the authors assume that the set of influenced pixels fall within the area limited by an ellipse. Hence, for the weights of the matrix W the following equation is applied:

$$w_{ij} = \frac{1}{\sqrt{LoS}} \begin{cases} \phi & \text{if } d_{ij}^1 + d_{ij}^2 < LoS + \lambda \\ 0 & \text{otherwise} \end{cases}$$

where LoS is the distance of the line of sight between two nodes, d_{ij}^1 and d_{ij}^2 are the distances from the centre of pixel j to the two node locations for link i, and λ is a tunable parameter describing the width of the ellipse. The parameter λ is typically set in the range from 0.1 to 0.6 m. The ellipse is primarily used to simplify the process of determining which pixels fall along the LoS (line of sight) path, as shown in figure 4, where grey pixels represent a person's body. Finally, the parameter ϕ is a scaling factor used to normalise the RTI, whose typical values are between 1 and 100 dB[2].

The model estimation of the values of RSS as a function of pixel in the equation (1) provides a mathematical framework to relate the target's movement in space to the RSS values per link. The model is an ill-posed inverse problem, that is, it is highly sensitive to measurement and modelling noise. The solution $\mathbf{s}_{px}$ can be calculated by the least-squares approach, but the solution can not be unique, hence a regularisation method [30] must be applied to obtain the solution. The method proposed by the authors propose is Tikhonov's regularisation. Using Tikhonov's method the least-squares problem is solved by

$$\hat{\mathbf{s}}_{px} = arg\min_{\mathbf{s}_{px}} \frac{1}{2}||W\mathbf{s}_{px} - \mathbf{s}||^2 + \alpha||Q\mathbf{s}_{px}||$$

where Q is the Tikhonov's matrix that produces the solution with the desired properties, and α is a tunable regularisation parameter. To calculate the parameter α many algorithms have been developed [31]. The least-squares problem solution is

$$\hat{\mathbf{s}}_{px} = (W'W + \alpha Q'Q)^{-1}W'\mathbf{s}. \tag{2}$$

As stated above, the matrix Q captures some features of the measured acquired. Taking into account the covariance matrix C as well as the variance σ_N^2 of the noise process linked to the measures, the solution of equation (2) can be calculated as

$$\hat{\mathbf{s}}_{px} = (W'W + \sigma_N^2 C^{-1})^{-1}W'\mathbf{s}. \tag{3}$$

The entries c_{ij} of the covariance matrix C can be calculated assuming that the spatial attenuation of the field decays exponentially [4]

$$c_{ij} = \sigma^2 exp\left(-\frac{d_{ij}}{\delta_c}\right)$$

where d_{ij} is the distance between centres of pixels i and j, σ^2 is the variance of pixel attenuation, and δ_c is a correlation parameter that can be used to determine the desired amount of smoothness in the image. The target's coordinates $\mathbf{x} = [x\ y]$ are the coordinates of the maximum value in the vector $\hat{\mathbf{s}}_{px}$ calculated by the regularisation method.

As stated above the authors propose two versions of the RTI-based algorithm, the first one evaluates RSS differences from the base situation, that is the RSS shadowing due to the target, and the second one evaluate the RSS variance. The solution shown in the equation (3) works in both cases, in fact, the only difference between two methods is how the entries of the vector $\mathbf{s}$ are evaluated. In the following we provide the descriptions of the ss entries calculation.

When using the Shadow-based method, for every link l, and every channel $c \in Ch$, average values of measured RSS values $\{\overline{RSS}_{lc}\}$ is computed when no target moves within the localisation area, this time is named calibration period. The method uses the $\overline{RSS}_{lc}$ values as a measure of the fade level following this rule: if $\overline{RSS}_{lc_1} < \overline{RSS}_{lc_2}$ then the link l is in a deeper fade in channel c_1 than in c_2. For each link l the $\overline{RSS}_{lc}$ values are sorted for all channels of the set C. Finally, the method creates a set $\mathcal{C}$ of size m containing the indices of the m highest channels by fade level, and then evaluates shadowing, that is the $\mathbf{s}$ entries as the mean values of the differences between the current measured RSS vales and the $\{\overline{RSS}_{lc}\}$, over the m highest channels by fade level.

For the Variance-based method the entries are the variances of the measured RSS values, and no calibration phase is needed.

In our experiments, variance is computed in a moving window whose length depends on the token speed, which is turn depends on the total numbers of anchors: from 264 ms in the case of 16 anchors to 408 ms for 24 anchors.

In [25], the authors describe an RTI-based tracking algorithm developed by filtering the estimated target positions through the Kalman filter defined as

$$\begin{aligned} \hat{V} &= V + \sigma_m^2 I_2; \\ G &= \hat{V}(\hat{V} + \sigma_n^2 I_2)^{-1} \\ \hat{\mathbf{x}} &= \hat{\mathbf{x}} + G(\mathbf{x} - \hat{\mathbf{x}}) \\ V &= (I_2 - G)\hat{V} \end{aligned}$$

where I_2 is the 2×2 identity matrix, σ_m^2 is the variance of the targets motion process, indicating how fast the object is capable of moving. Larger values enable the filter to track faster moving objects. The authors also take into account σ_n^2 that is the variance of the measurement noise. Larger values will cause the filter to

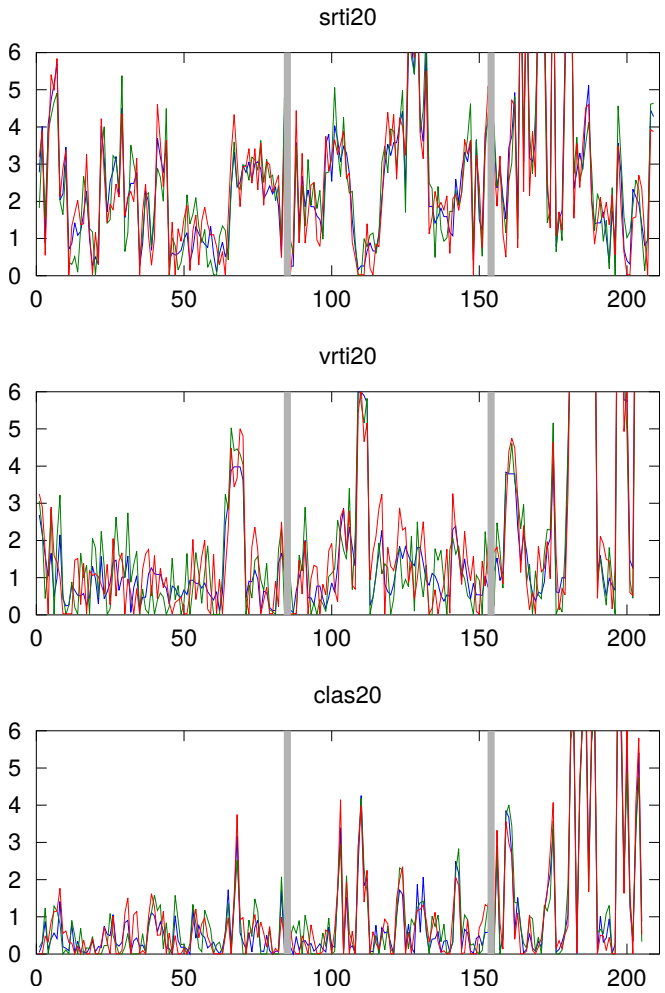

Fig. 5: Error in metres for three algorithms over the 211 positions. The three coloured lines represent different repetitions of the same experiment.

trust more the statistical predictions over the instantaneous measurements. The vector $\hat{\mathbf{x}}$ contains the Kalman estimated coordinates x and y. $\mathbf{x}$ is a two-element vector containing the instantaneous measurement of the target coordinates through the RTI method. $\hat{V}$ is the a priori error covariance matrix and V is the posterior error covariance matrix and finally G the Kalman Gain. The authors provide some values for these parameters through a set of measurements performed during their experiments.

5 Results and discussion

We made a total of 3 *measurements*, with 24, 20 and 16 anchors hanging from the walls. Each measurement, as detailed previously, consisted of 3 *repetitions* of 211 *positions*, for a total of 633 *samples* on each of which the positioning *error* was computed. While the total amount of samples is small in a statistical sense, in the following we are going to explain why we think our results are credible.

We define a total of nine *situations*, each relative to one of the three measurements (24, 20 and 16 anchors) for each of the three *algorithms* we have used, that is an SVM classifier (CLAS), the shadow-based radio tomographic imaging (SRTI) and the variance-based one (VRTI). This way, we can make a comparison of the relative accuracy performance of the three algorithms with different number of anchors.

Each measurement was repeated three times, both for obtaining a higher number of error samples and making statistics more reliable, and for being able to make a direct comparison between the *repetitions* along all the 211 positions of the path. Each of the three plots of figure 5 shows a different-coloured line for each of the three repetitions: the three superimposed lines exhibit clear indications of statistical noise and a strong spatial correlation between them, that is, between repetitions. We consider this spatial correlation a good indication of the robustness of the experimental procedure. Additionally, to a lesser extent, we can observe spatial correlation also among the different algorithms, suggesting that in the specific anchor configuration used in this measurement some positions points provide low-quality information. The fact that in many instances this translates in poor performance for all the three algorithms is an additional indication of the robustness of the experimental procedure.

The three measurements and the three repetitions were done in a completely independent way, at time distances of some hours to some days.

5.1 Overall comparison of the three algorithms

In figure 6 we show the error distributions for the nine situations. For easier comparison, the distributions are overlaid with four performance indicators, namely the root of mean square (RMS) error and the 50^{th}, 75^{th} and 90^{th} percentiles of errors.

From a practical standpoint, the 75^{th} percentile is the most useful estimator, and indeed it is the one that has been used in the indoor localisation track of the EvAAL competition [32]. The 90^{th} percentile is useful to get an idea of the length of the tail of the error distribution, while the median and RMS errors are useful for comparison with statistics found in the literature.

It is apparent from figure 6 how CLAS outperforms the tomography-based methods in terms of pure error performance. This was to be expected, given given that CLAS is classification-based, and it exploits prior knowledge that is not available to the other algorithms. This knowledge comes at a significant cost both in terms of installation and of flexibility. More specifically, the training phase requires non-negligible time to be performed by a person following a rigid protocol, and a new training is required for any non-trivial change in the environment, such as a rearrangement of furniture. This is not something that is reasonably done by the end user, and probably rules out the usage of this system for some typical scenarios. For installation in private homes (common in AAL scenarios), the intervention of a technician would be required every time that furniture is reallocated. Even in places where technicians are promptly available, the required intervention rate could turn out to be prohibitive in dynamic environments, such as hospitals or industrial locations, where furniture can be expected to be routinely moved around. The time required for CLAS training by a qualified technician is about 5 s per cell, with squared cells of edge 0.6 metres, for an overall 8 s/m^2 plus overhead for setup and testing.

SRTI has the worst error performance. On the other hand, it needs a calibration phase which is much quicker than the training needed by CLAS and which can be completely automated, requiring no human intervention. In practice, when the system senses no motion in the environment for some time, it can autonomously initiate a recalibration procedure that lasts for a few minutes, and is automatically cancelled if any movement is detected in the meantime.

VRTI is midway. It does not need any training phase, because it is not sensitive to unmoving obstacles, and as such it is insensitive to changes in the environment. This strength is also its main weakness: being based on signal strength variations, it performs badly when the target does not move. Note, however, that here we are measuring the performance of the *raw* system: by adding a tracking layer with memory, such as a Kalman filter or a particle filter, we can expect performance to improve significantly with non-moving targets.

Table 1 summarises the main characteristics of the three algorithms; *accuracy* is the 75^{th} percentile of error in the 24-anchors measurement, which we consider the most appropriate metrics for an experimental localisation algorithm.

The CLAS algorithm gives a higher accuracy than the others, however it requires an expensive calibration procedure making it not ideal for the application scenarios typical of the AAL domain. When

Table 1 Functional comparison of the three algorithms.

Performance indicator	**SRTI**	**VRTI**	**CLAS**
Accuracy	1.9 m	1.5 m	1.2 m
Configuration	automated	unneeded	expensive
Still target	detected	undetected	detected
Flexibility	yes	yes	no
Reference scenario	AAL, industrial, intrusion, hospital	same as SRTI	specific applications

changes in the localisation area are sporadic, the CLAS algorithm can be adopted. However, in these cases, when installing additional anchor devices is tolerable, other device-free technologies (such as infrared, ultra-wideband, cameras etc...) are good candidates, especially because they require few anchors and can provide high accuracy.

On the other hand, SRTI and VRTI algorithms fit best in many scenarios where the targets move often and where the localisation application does not demand high accuracy.

For all the algorithms, the accuracy of the estimation increases with the number of anchors, but it is still in the usable range with as few as 16 anchors. This observation is an interesting result because, to the best of our knowledge, up to now the literature lacks studies on the influence of the placement and number of anchors on the accuracy of the device-free methods based on RSS which are the focus of this paper. In the next section we examine this topic in deeper detail.

5.2 Dependence on the number of anchors

While the data shown so far seem to indicate that dependency of the accuracy from the number of anchors is consistent, it is important to note that placement of anchors can have a significant effect, which is difficult to gauge. The reason is that, even for a single environment, the space of possible placements of a fixed number of anchors is huge, and it is not clear how to experimentally choose a meaningful part of this space. We have then exploited the fact that, for each measurement, considering a subset of the anchors effectively creates a new *configuration* of anchor placements.

For each of the three measurements, we remove the data relative to progressively more anchors. For example, we compare the performance of the three algorithms with 24 anchors with that obtained when one anchor is ignored, that is, with a 23-anchors configuration. There are 23 possible such configurations, one anchor being the sync and as such not possibly being ignored. Analogously, by ignoring two anchors, we can compute what is the performance in a given situation with a 22-anchors configuration: there are $23\dot{2}2/2$ possible such configurations.

Using this trick, we can obtain the performance of the system with progressively fewer anchors. Moreover, since there are many subsets of 24 anchors, we also obtain an interval of performance values for the same number of anchors, corresponding to many different anchor placement configurations.

Note that this procedure is conservative as far as the localisation performance is concerned. In fact, starting from a 24-anchors configuration and ignoring the output of 8 anchors is the same as starting

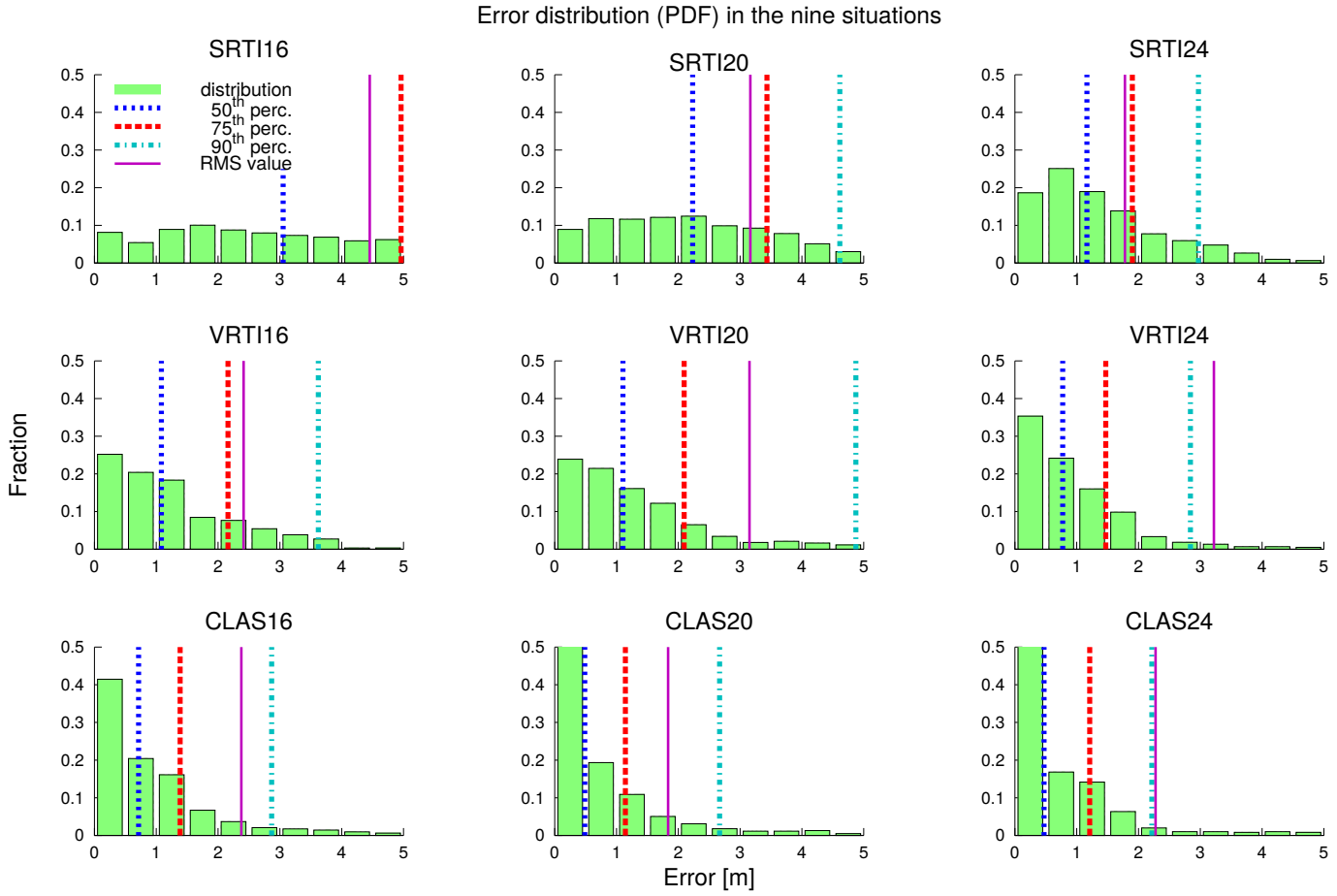

Fig. 6: Distribution of errors in the nine situations with superimposed statistics of RMS error and 50th, 75th and 90th error percentiles.

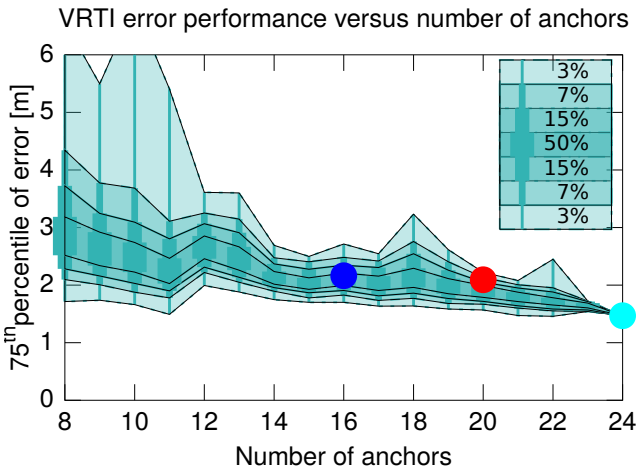

Fig. 7: Error performance (75th percentile of error) for 10111 different anchor configurations. A variable number of anchors is ignored starting from the 24-anchors measurement. The red and blue dots represent the 20- and 16-anchors measurements.

Table 2 Number of anchor configurations for the VRTI case with 24 initial anchors.

Anchors	Configurations
24	1
23	23
22	253
21	286
20	495
19	792
18	924
17	330
16	1287
15	220
14	900
13	900
12	900
11	700
10	700
9	700
8	700

from the remaining 16 anchors. However, one should remember that the experimentation uses a token-passing protocol, and the speed at which the token completes a cycle is lower in the 24-anchor situation with respect to a 16-anchor configuration. This means that in the first case the localisation algorithm will profit from a lower number of samples, which justifies the observation that our procedure is conservative, at least in principle.

As an initial example, let's use the VRTI algorithm in the 24-anchors measurement. We use the 75th percentile of error as a performance measure. In figure 7 we depict the performance of a total of 10111 different anchor configurations chosen from all the possible configurations of 24 anchors with some of them disabled, as detailed in table 2. We have not considered all possible configurations, because of computing power constraints and because many of them do not make sense. In fact, we use the whole sets for the 24, 23 and 22 cases, while for the remaining cases we only considered those configurations where the anchors removed from the initial set of 24 were not too near to each other. For configurations with less than 15 anchors, among the candidate reasonable configurations we randomly picked a fixed number, for computation performance reasons. The figure shows different shaded regions separated from percentiles lines of 0, 3, 10, 25, 75, 90, 97, 100, thus summarising the performance of all the considered configurations, where again the performance measure is the 75th percentile of error, which we consider the most significant and robust [32].

Figure 7 is interesting in a number of ways. First of all, consider the inner area, the darkest one which starts with the vertex at 24 anchors and grows progressively wider with diminishing number of anchors. This is the area where 50% of cases fall. This means that, when removing anchors from the whole 24-anchors configuration, in half of cases the 75th percentile of error is inside this area. Notice how the area gently slopes towards greater errors with diminishing number of anchors: this is a very strong indication that the VRTI method behaves smoothly when reducing the number of anchors from the high figures usually found in the literature, meaning that with this method it is possible to consider trade offs between localisation accuracy and number of installed devices. This is the most important finding of this paper.

Second, the results are consistent within the experiment: looking at the lightest areas on top, one sees that significant deviations from the most common performance measure are found in only 3% or 10% of cases. This means that in the vast majority of cases, the way the anchors are placed in the environment is not that important, assuming that one does not install devices in bunches. This is the second most important finding of this paper.

Third, the regular shape of the plot is one more confirmation of the robustness of our measurement method. A further confirmation is given by the position of the red and blue dots, which represent the 75th percentile of error of the VRTI measurements with 20 and 16 anchors respectively. Since the results represented by the red and blue dots are relative to different experiments, made at different times with different device positions, having them inside the areas including 80% and 50% of configurations, respectively, means that not only the computation method is consistent within data from an experiment, but even across experiments.

Having examined in detail the configurations stemming from VRTI in a single measurement, we can comment figure 8, where a single picture summarises the performance of all the configurations stemming from the three algorithms in the three measurements. The same observations as above apply here for each of the nine plots and each of the three coloured areas the plots. The areas are delimited by the 10th and 90th percentiles of the performance measure; in other words, in 80% of the anchor configurations, the performance measure (75th percentile, root mean square or 90th of error) falls inside the coloured area. Note that the vertical scale is not the same for all algorithms.

Figure 8 shows that in almost all cases the measurement obtained in the 20-anchors measurement (vertex of the pink area) falls within the cyan area, and the measurement for the 16-anchors measurement (vertex of the violet area) falls within both other areas. The exceptions are all for 90th percentile error performance measure, which is not as robust as the two other ones. This observation is still a confirmation of the good consistency of our measurements and of our procedure of removing anchors to produce new configurations with a variable number of anchors.

Even more interesting is the fact that the graceful degradation of performance with diminishing number of anchors that we had observed in figure 7 can be observed in all situations, with the partial exception of the CLAS algorithms. This brings us to two important results: for all performance measures (75th percentile, root mean square and 90th of error), all three algorithms can 1) be used with smaller numbers of anchors than normally used in the literature, at the price of a gradual loss of accuracy, and 2) all three algorithms are relatively insensitive to the positioning of anchors in the environment.

The strange zigzag behaviour of the CLAS method observed in figure 8 should probably be attributed to peculiarities of the paths 2 and 3. In fact, when considering only Path 1, the behaviour is much more regular for all performance measures, as shown in figure 9 for the 75th percentile of error. CLAS, being a classification-based algorithm is also strongly non-linear, more so than the tomography-based ones. This may explain both the irregular behaviour and the increased loss of performance with less than 12 anchors.

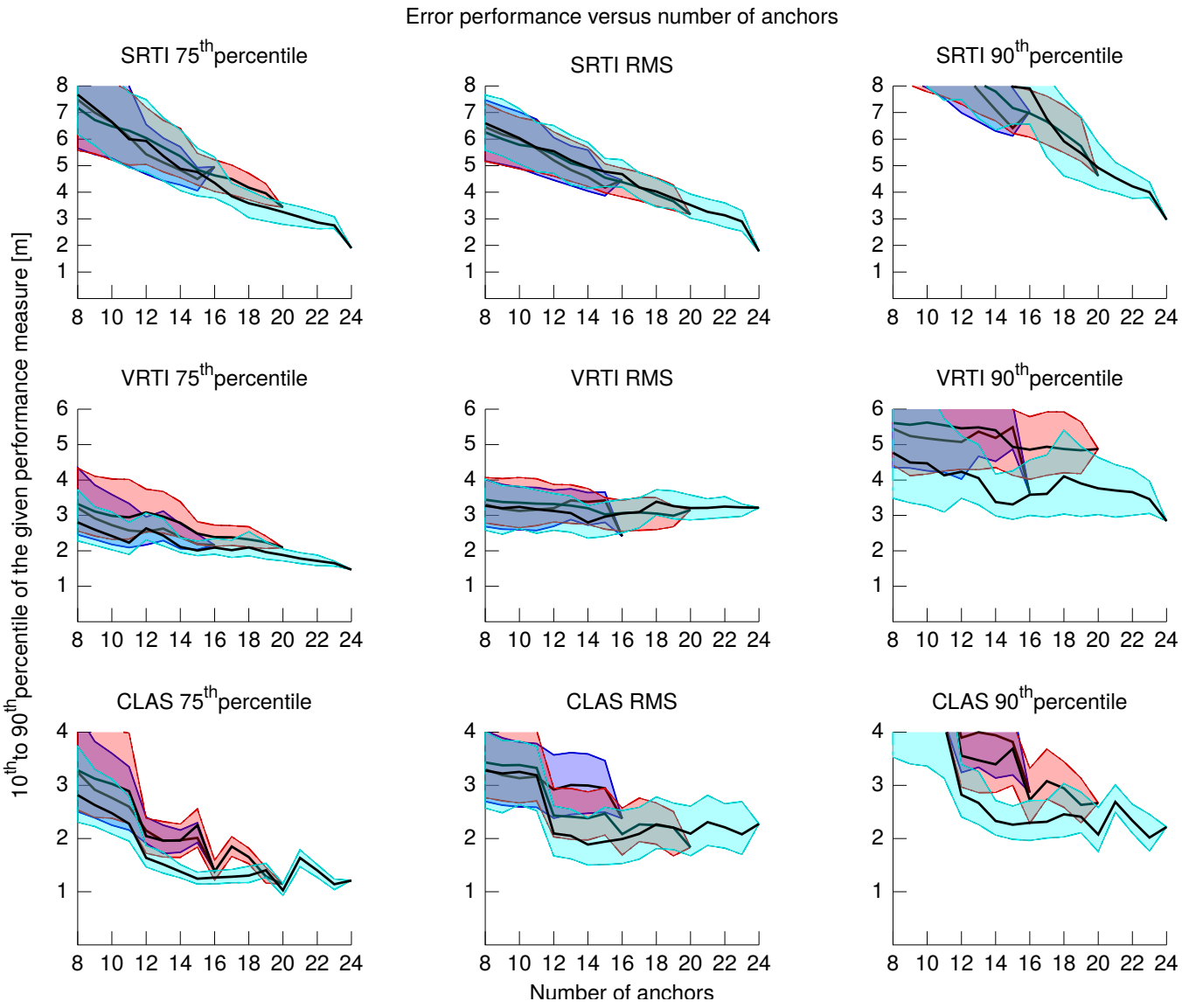

Fig. 8: Error performance according to three different performance indicators for the three algorithms versus number of anchors. Many anchor configurations are obtained starting from the 24-, 20- and 16-anchors measurements.

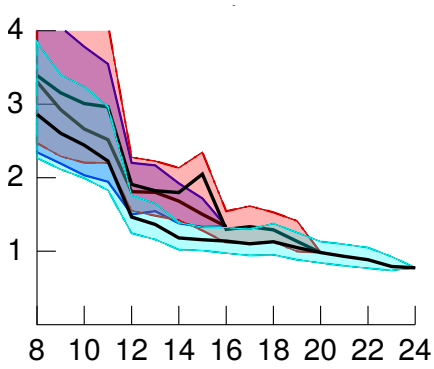

Fig. 9: Same as figure 8 but only for Path 1. Only the CLAS method with 75th percentile performance measure is shown.

6 Conclusion and open research problems

We have compared three RSS-based device-free indoor localisation methods belonging to two different families and we have compared their relative merits in a realistic environment through rigorous experimentation.

We have presented three novel results: first, these methods can be used with much less transmitters than normally found in the literature, which makes them a possibly good choice in a future IoT pervasive scenario.

Second, these methods degrade their performance gracefully with diminishing number of sensors, which makes it possible to trade accuracy for number of active devices. This characteristic too makes them a palatable choice for a scenario where small, low-power, ubiquitous devices can be used, at no hardware or installation cost, as an indoor localisation infrastructure.

Third, the systems that we have considered are largely insensitive to the exact positioning of devices in the environment, as long as they are not installed in bunches.

In order for these methods to be in fact usable in a pervasive IoT scenario, the next step is to verify what is the performance in the case of intermittent operation of heterogeneous transmitters. In fact, the "parasitic" usage of IoT transmissions implies that the methods need to work with a possibly high number of different-technology devices, each transmitting with a generally low or very low duty cycle.

Furthermore, while the computing power required from the devices is indeed very low at transmission time, they however need to listen to other devices' transmission, which is power-hungry. No obvious solutions to this problem exist, but many avenues could

be investigated, for example some form of passive listening or transmission synchronisation.

Acknowledgment

This work was supported by Regione Toscana under the European Union research funding program POR CRO FSE 2007-2013 and by the project "Energia da fonti rinnovabili e ICT per la sostenibilità energetica; sottoprogetto Smart Building" of the DIITET Department of CNR.

7 References

1 Dohr, A., Modre.Opsrian, R., Drobics, M., Hayn, D., Schreier, G. 'The internet of things for ambient assisted living'. In: Information Technology: New Generations (ITNG), 2010 Seventh International Conference on. (, 2010. pp. 804–809
2 Wu, P., Wu, X., Chen, G., Shan, M., Zhu, X.: 'A few bits are enough: Energy efficient device-free localization', *Computer Communications*, 2016, **83**, pp. 72 – 80
3 Wu, P., Chen, G., Zhu, X., Wu, X.: 'Minimizing receivers under link coverage model for device-free surveillance', *Computer Communications*, 2015, **63**, pp. 53 – 64
4 Ossi, K., Bocca, M., Patwari, N. 'Enhancing the accuracy of radio tomographic imaging using channel diversity'. In: IEEE Int. Conf. MASS. (Las Vegas, Nv, 2012. pp. 1–9
5 Viani, F., Martinelli, M., Ioriatti, L., Benedetti, M., Massa, A. 'Passive real-time localization through wireless sensor networks'. In: Proc. IEEE Intl. Conf. IGARSS. (Cape Town, South Africa, 2009. pp. 718–721
6 J. Wilson and N. Patwari: 'Radio Tomographic Imaging with Wireless Networks', *IEEE Transaction on Mobile Computing*, 2010, **9**, (5), pp. 621–632
7 Cassarà, P., Potortì, F., Barsocchi, P., Girolami, M. 'Choosing an RSS device-free localization algorithm for ambient assisted living'. In: proceedings of the International Conference on Indoor Positioning and Indoor Navigation (IPIN). (, 2015.
8 Valtonen, M., Maentausta, J., Vanhala, J. 'Tiletrack: Capacitive human tracking using floor tiles'. In: Pervasive Computing and Communications, 2009. PerCom 2009. IEEE International Conference on. (, 2009. pp. 1–10
9 Krumm, J., Harris, S., Meyers, B., Brumitt, B., Hale, M., Shafer, S. 'Multi-camera multi-person tracking for easyliving'. In: Visual Surveillance, 2000. Proceedings. Third IEEE International Workshop on. (, 2000. pp. 3–10
10 Patel, S.N., Reynolds, M.S., Gregory.D..Abowd", J. editor="Indulska, Patterson, D.J., Rodden, T., Ott, M. In: 'Detecting human movement by differential air pressure sensing in hvac system ductwork: An exploration in infrastructure mediated sensing'. (Berlin, Heidelberg: Springer Berlin Heidelberg, 2008. pp. 1–18
11 Barsocchi, P., Potortì, F., Nepa, P. 'Device-free indoor localization for aal applications'. In: International Conference on Wireless Mobile Communication and Healthcare. (Springer, 2012. pp. 361–368
12 Fink, A., Beikirch, H. 'Device-free localization using redundant 2.4 GHz radio signal strength readings'. In: Indoor Positioning and Indoor Navigation (IPIN), 2013 International Conference on. (, 2013. pp. 1–7
13 Savazzi, S., Nicoli, M., Carminati, F., Riva, M.: 'A bayesian approach to device-free localization: modeling and experimental assessment', *IEEE Journal of Selected Topics in Signal Processing*, 2014, **8**, (1), pp. 16–29
14 Savazzi, S., Nicoli, M., Riva, M. 'Radio imaging by cooperative wireless network: Localization algorithms and experiments'. In: Proc. IEEE Intl. Conf. WCNC. (Paris, France, 2012. pp. 1–5
15 C. Morelli, M. Nicolini, V. Rampa, and U. Spagnolini: 'Hidden Markov Models for Radio Localization in Mixed LOS/NLOS Conditions', *IEEE Transaction on Signal Processing*, 2007, **5**, (4), pp. 1525–1542
16 Wagner, B., Striebing, B., Timmermann, D. 'A system for live localization in smart environments'. In: Proc. IEEE Intl. Conf. ICNSC. (Evry, France, 2013. pp. 684–689
17 Wagner, B., Patwari, N., Timmermann, D. 'Passive rfid tomographic imaging for device-free user localization'. In: Proc. IEEE Intl. Conf. WPNC. (Dresden, Germany, 2012. pp. 120–125
18 Nannuru, S., Li, Y., Zeng, Y., Coates, M., Yang, B.: 'Radio-frequency tomography for passive indoor multitarget tracking', *IEEE Transactions on Mobile Computing*, 2013, **12**, (12), pp. 2322–2333
19 Wang, J., Gao, Q., Yu, Y., Cheng, P., Wu, L., Wang, H.: 'Robust device-free wireless localization based on differential rss measurements', *IEEE Transactions on Industrial Electronics*, 2013, **60**, (12), pp. 5943–5952
20 Men, A., Xue, J., Liu, J., Xu, T., Zheng, Y. 'Applying background learning algorithms to radio tomographic imaging'. In: Proc. IEEE Intl. Conf. WPMC. (Atlantic City, NJ, 2013. pp. 1–5
21 Maas, D., Wilson, J., Patwari, N. 'Toward a rapidly deployable radio tomographic imaging system for tactical operations'. In: Proc. IEEE Intl. Workshop SenseApp. (Sydney, Australia, 2013. pp. 1–8
22 Zhao, Y., Patwari, N., Suresh, J.M.P. 'Radio tomographic imaging and tracking of stationary radio tomographic imaging and tracking of stationary and moving people via kernel distance'. In: Proc. ACM Intl. Conf. IPSN. (Philadelphia, Pennsylvania, USA, 2013. pp. 1–12
23 Crossbow Technology. 'IRIS Datasheet'. (, 2013. `http://bullseye.xbow.com:81/Products/productdetails.aspx?sid=264`
24 Wilson, J., Patwari, N.. 'Spin: A token ring protocol for RSS collection'. (, . http://span.ece.utah.edu/spin
25 Wilson, J., Patwari, N.: 'See-through walls: Motion tracking using variance-based radio tomography networks', *Mobile Computing, IEEE Transactions on*, 2011, **10**, (5), pp. 612–621
26 Press, W.H., Teukolsky, S.A., Vetterling, W.T., Flannery, B.P.: 'Numerical Recipes'. (Cambridge University Press, 2007)
27 Vapnik, V.: 'Statistical Learning Theory'. (New York: Wiley, 1998)
28 A. Massa, A. Boni and M. Donelli: 'A Classification Approach Based on SVM for Electromagnetic Subsurface Sensing', *IEEE Tran On Geoscience and Remote Sensing*, 2005, **43**, (9), pp. 2084–2093
29 Platt, J.: 'Probabilistic outputs for support vector machines and comparison to regularized likelihood methods'. (Cambridge, MA: Advances in large margin Classifiers, MIT Press, 1999)
30 Wilson, J., Patwari, N., Vasquez, F.G. 'Regularization methods for radio tomographic imaging'. In: Proc. Virginia Tech Wireless Symposium. (Virginia, USA, 2009. pp. 1–9
31 Engl, H.W., Hanke, M., Neubauer, A.: 'Regularization of Inverse Problems'. (SPRINGER, 2004)
32 Barsocchi, P., Chessa, S., Furfari, F., Potortì, F.: 'Evaluating AAL solutions through competitive benchmarking: the localization competition', *IEEE Pervasive Computing Magazine*, 2013, **12**, (4), pp. 72–79